Computer Methods and Programs in Biomedicine 230 (2023) 107350

Contents lists available at ScienceDirect

Computer Methods and Programs in Biomedicine

journal homepage: www.elsevier.com/locate/cmpb

Insights from an electro-mechanical heart failure cell model: Role of SERCA enhancement on arrhythmogenesis and myocyte contraction

Maria Teresa Mora[a], Antonio Zaza[b,c], Beatriz Trenor[a,*]

[a] Centro de Investigación e Innovación en Bioingeniería, Universitat Politècnica de València, Valencia, Spain
[b] Dipartimento di Biotecnologie e Bioscienze, Università degli Studi Milano-Bicocca, Italy
[c] Unità di Fisiologia Cardiovascolare, IRCCs Istituto Auxologico Italiano, Italy

ARTICLE INFO

Article history:
Received 26 September 2022
Revised 27 December 2022
Accepted 10 January 2023

Keywords:
Heart failure
Electro-mechanics
Computational modeling
Twitch force
Early afterdepolarizations
SERCA

ABSTRACT

Background and objective: Structural and electrical remodeling in heart failure predisposes the heart to ventricular arrhythmias. Computer modeling approaches, used to complement experimental results, can provide a more mechanistic knowledge of the biophysical phenomena underlying cardiac pathologies. Indeed, previous in-silico studies have improved the understanding of the electrical correlates of heart failure involved in arrhythmogenesis; however, information on the crosstalk between electrical activity, intracellular Ca^{2+} and contraction is still incomplete. This study aims to investigate the electro-mechanical behavior of virtual failing human ventricular myocytes to help in the development of therapies, which should ideally target pump failure and arrhythmias at the same time.

Methods: We implemented characteristic remodeling of heart failure with reduced ejection fraction by including reported changes in ionic conductances, sarcomere function and cell structure (e.g. T-tubules disarray). Model parametrization was based on published experimental data and the outcome of simulations was validated against experimentally observed patterns. We focused on two aspects of myocardial dysfunction central in heart failure: altered force-frequency relationship and susceptibility to arrhythmogenic early afterdepolarizations. Because biological variability is a major problem in the generalization of in-silico findings based on a unique set of model parameters, we generated and evaluated a population of models.

Results: The population-based approach is crucial in robust identification of parameters at the core of abnormalities and in generalizing the outcome of their correction. As compared to non-failing ones, failing myocytes had prolonged repolarization, a higher incidence of early afterdepolarizations, reduced contraction and a shallower force-frequency relationship, all features peculiar of heart failure. Component analysis applied to the model population identified reduced SERCA function as a relevant contributor to most of these derangements, which were largely reverted or diminished by restoration of SERCA function alone.

Conclusions: These simulated results encourage the development of strategies comprising SERCA stimulation and highlight the need to evaluate both electrical and mechanical outcomes.

Abbreviations

AP	action potential
APD	action potential duration
CaT	Ca^{2+} transient
CaTA	Ca^{2+} transient amplitude
DevF	developed force
EAD	early afterdepolarization
EMw	electro-mechanical window
FFR	force-frequency relationship
HF	heart failure
SR	sarcoplasmic reticulum
TTP	time to peak force
RT	recovery time.

1. Introduction

Cardiovascular diseases are the leading cause of mortality worldwide and the incidence of heart failure (HF), eventually their common fate, is increasing due to population aging. Reduced ejection fraction and electrical instability are the most damaging con-

* Corresponding author.
E-mail address: btrenor@eln.upv.es (B. Trenor).

https://doi.org/10.1016/j.cmpb.2023.107350

sequences of HF; ideally, treatments should address them both. However, therapeutic efficacy can vary between patients due to genotype differences, suggesting the need to consider intrinsic variability in studies.

The complexity of biological systems makes integration of specific experimental findings into disease patterns very difficult. Currently, mathematical biophysical models are widely used to fill this gap; they provide a powerful tool for mechanistic interpretation and prediction, the latter including the virtual test of pharmacological compounds. Most previous in-silico investigations focus on electrophysiology [1–3], however, excitation and contraction closely interact and abnormalities in both coupled processes in HF determine the disease pattern. The development of myofilament contraction models [4,5], and more recently with human data [6], allows the integration of cellular mechanics with the electrical part. Indeed, this electro-mechanical approach has contributed to the understanding of arrhythmogenesis triggered by oscillations in action potential duration, alternans, or drugs [7–10], but not in the setting of HF.

Both structural and functional changes contribute to the propensity for ventricular arrhythmias in HF. Altered transcription and/or post-transcriptional modification (e.g. phosphorylation) account for abnormality of channel and transporters function, which are also affected by disruption of membrane microdomains [11]. Among them, the loss of transverse tubules (T-tubules) has remarkable consequences on Ca^{2+} dynamics because of loss of the spatial relationship between L-type calcium channels (LTCC), ryanodine receptors (RyRs), and Na^{+}/Ca^{2+} exchangers (NCX). Models incorporating all these factors allow to reproduce the observations in failing myocytes more accurately and obtain more realistic predictions.

Cardiac contractile reserve assures myocardial contraction with changes in heart rate, however it is impaired in HF. The relationship between heart rate and developed force (force-frequency relationship, FFR) depends on the competition between several Ca^{2+} fluxes; thus, its steepness ("slope") integrates the function of the main cellular Ca^{2+} transports and buffers. Normally positive in the human heart, FFR slope is reduced, or even inverted, in HF [12,13]. Interestingly, increased susceptibility to arrhythmias has been correlated with negative FFR [14]. Early afterdepolarizations (EADs) are a frequent arrhythmogenic mechanism in HF and they are an integrated phenomenon as well, resulting from the crosstalk between sarcolemmal conductances and intracellular Ca^{2+} dynamics.

We used, for the first time, a comprehensive electro-mechanical single-cell model to assess which among the abnormalities described in HF may mostly contribute to contractile deficit, FFR depression and arrhythmogenesis by EADs. The "electromechanical window" (EMw) a clinically measurable parameter reported to quantify arrhythmogenic risk [15] was also considered. Computational simulations were performed using a population-based approach, wherein a population of models is obtained by implementing variability of input parameters to produce a spectrum of phenotypes recapitulating biological variability. Variability of model output (electro-mechanical responses) allowed identification of influential input parameters by using statistical criteria, which would be impossible with a fully deterministic approach.

2. Methods

2.1. Electro-mechanical model of heart failure

A widely accepted human action potential model, the ToR-ORd model [16], which includes 14 ionic currents for electrophysiology and intracellular Ca^{2+} dynamics, was selected to be coupled to an active force (sarcomere) model [6] to fully simulate excitation-contraction (EC) coupling and mechano-electrical feedback, exactly as recently done in [10], where some mechanical parameters were re-adjusted to improve the outputs of the human model. When integrating both models, intracellular Ca^{2+} acts as the intermediate agent between the electrical and the mechanical activity. The model includes the dyadic subspace, an intracellular microenvironment resulting from contiguity of the sarcolemmal and sarcoplasmic reticulum (SR) membranes, essential in the interaction between the effectors of EC-coupling. The dyadic space (defined by the subscript 'ss') and the bulk cytosolic compartment (defined by the subscript 'i') were analyzed separately, an approach that proved essential in mechanism interpretation (see below). Stretch-activated sarcolemmal channels were also included in the model for completeness; however, they are inconsequential in the present work because the simulations were performed under isometric conditions. MATLAB code of ToR-ORd model [16] was used as the basis to implement all the modifications.

The electro-mechanical model was applied to generate virtual "control" (considered healthy) and "failing" myocytes. The HF myocyte was obtained by introducing in the healthy one the electrophysiological remodeling changes detailed by Gomez et al. [17] (Supplementary Table S1), molecular changes observed in failing myocytes extracted from hearts with reduced ejection fraction. In brief, SERCA maximal flux velocity was downregulated by 55% and NCX one upregulated by 60%, Ca^{2+} leak from the SR compartment (SR leak) increased by 30% and RyRs channel sensitivity to SR Ca^{2+} increased ($K_{rel,Ca}$ was reduced by 20%). Ion currents were also affected by HF: the conductance of I_{NaL} (represented as an independent component), was upregulated by 30% and its time constant τ_{hL} was increased by 80%, I_{to}, I_{K1} and I_{NaK} conductances were downregulated by 60%, 32%, and 30%, respectively. Finally, CaMK activity was increased by 50%.

Furthermore, loss of T-tubules, a functionally relevant feature of cellular remodeling, was introduced in the HF model accordingly to Sanchez-Alonso et al. observations [18]. T-tubular structure reduction partially disrupted the dyadic space, redistributing part of LTCC and NCX proteins from the dyadic sarcolemma to that delimiting the bulk cytosolic space. As a consequence, part of the Ca^{2+} release units (LTCC-RyR pairs) were uncoupled, thus increasing the proportion of "orphaned" RyR channels. In addition, based on experimental findings in myocytes with dilated cardiomyopathy [18], LTCCs located in the sarcolemma were maximally phosphorylated by CaMKII. Exact details about the implementation of these changes in the myocyte model can be found in the Supplementary Material.

Heart failure remodeling also affects the contractile apparatus, being the elevation of myofilament Ca^{2+} sensitivity the most common alteration. According to experimental observations [19,20], this change in Ca^{2+} sensitivity was modeled by reducing by 30% the Ca^{2+} concentration required for half-maximal Troponin C binding ($[Ca]_{T50}$ in Land et al. [6]).

All simulations were performed in MATLAB (R2020b, MathWorks) and were run on endocardial-type cells at steady state stimulation (i.e. after 500 beats in each condition). Active force was obtained under isometric conditions, i.e. with no changes in sarcomere length.

2.2. Population of models

To account for biological variability and experimental uncertainty, our analysis was based on the comparison between populations of "myocytes" (i.e. models). To this end, an initial population of 1000 healthy myocytes was generated by randomly applying scaling factors to a total of 29 parameters (18 of channels/transporters and 11 of sarcomeric proteins, see Supplementary Tables S2 and S3) to the baseline model, so that each myocyte had a different set of randomly combined parameters. We assumed

that parameters were normally-distributed and they had the same standard deviation to control variability across parameters. Setting a standard deviation of 0.15 for all parameters was necessary to obtain a sufficiently large model population with both electrical and mechanical features compatible with experimentally observed features. The scaling factors followed thus a normal distribution with a mean equal to 1 and a standard deviation of 0.15. System complexity led to a large number of interactions between parameter changes, which add to parameter variability in determining output variability. As a consequence, the chosen range of parameter variability led to a very broad population of outputs, whose boundaries exceeded experimentally observed values. Thus, model refinement was performed by eliminating profiles out of boundaries for healthy myocytes, leading to a population of 190 models whose output matched experimentally observed values of electrophysiological and mechanical properties listed in Tables S4 and S5. See supplementary material for additional details. The HF myocyte population was generated from the healthy one by changing the parameters scaling factors as detailed in the previous paragraph. Model refinement was applied to this population by eliminating profiles characterized by values exceeding ± 3 SD from the population mean. The remaining 190 models had electrophysiological and mechanical properties consistent with the heterogeneities among experiments (Tables S6–S8).

As opposed to comparison between fully deterministic models, the comparison between model populations allows to extract significant parameters by statistical methods. This makes simulations outcome robust with respect to natural variability, thus increasing its predictive value.

2.3. Biomarkers in model output

The following electrophysiological, Ca^{2+} handling and mechanical properties (biomarkers) were measured during stimulation at steady-state in each condition: action potential duration at 90% of repolarization (APD_{90}), cytosolic Ca^{2+} transient (CaT) amplitude (CaTA) and developed force (DevF), calculated as the difference between systolic and diastolic Ca^{2+} and force values respectively, time to peak force (TTP), and times at 50% and 90% recovery from peak force (RT_{50} and RT_{90}). CaT duration was measured at 80% of decay ($CaTD_{80}$); total duration of the force twitch, including contraction and relaxation, was calculated as TD_{90}=TTP+RT_{90}. For quantification of the electromechanical window (EMw), i.e. the difference between the duration of the mechanical and electrical systoles, we used TD_{90} and APD_{90} (EMw=TD_{90}-APD_{90}). The total net charge transferred during repolarization (Q_{Total}) was obtained by integrating the total membrane current (algebraic summation of individual currents) after the AP upstroke. Q_{Total} was normalized to APD_{90} (Q_{Total}/APD), thus obtaining an index corresponding to the mean value for net membrane current over repolarization.

We used vulnerability to EADs as a marker of electrical instability. The protocol to this end included an EAD-inducing "perturbation" consisting of a lower stimulation frequency (0.25 Hz) and decreased I_{Kr} conductance (to simulate the effect of dofetilide), as in Margara et al. [10] study. A 40% reduction in I_{Kr}, emulating the decrease caused by 0.01 μM dofetilide, provided the suitable conditions to induce EADs in failing myocytes but not in the healthy ones.

3. Results

3.1. From an in silico heart failure electro-mechanical cellular model to a virtual population

The integration of cellular mechanics in the action potential model of a ventricular myocyte allowed to explore the whole excitation-contraction coupling process that starts with the electrical activation of cell membrane and leads to a contraction force, being Ca^{2+} the intermediate agent. Fig. 1 compares action potential (AP), Ca^{2+} transient (CaT) and active force in healthy (black) and failing (red) cardiomyocytes at 1 Hz. The three upper panels represent the output with the mean value of parameters in each condition (baseline models). HF myocytes had prolonged APD, smaller and slower CaT, leading to smaller and slower contraction/relaxation. Notably, the reduction in force did not match the one of CaT, reflecting the increment in myofilament sensitivity to Ca^{2+}. These differences observed between healthy and failing myocytes at 1 Hz were more relevant at larger heart rates, particularly in developed force (see next section).

Fig. 1B compares the healthy population of 190 myocytes with the failing one, i.e. it includes variability in profiles. Albeit the same parameter variability was applied to both model populations, profiles variability differed between the healthy and HF population.

Firstly, within each condition, variability was larger for mechanical than for electrophysiological outputs (Supplementary Fig. S2). Indeed, mechanical constraints dominated in restricting the initial population of 1000 models to that producing outputs within the physiological range. Notably, there was not a specific range of mechanical parameters leading to physiological phenotypes; mechanical responses varied instead as a consequence of multiple interactions between model parameters. This suggests that the excitation-contraction coupling process has a higher degree of non-linearity (complexity) as compared to excitation itself.

APD_{90}, $CaTD_{80}$, and TD_{90} values, represented in Fig. 2, were larger in failing than in healthy myocytes and variability within the population increased in the HF one. The EMw was also prolonged in HF because the force transient was more prolonged than APD. EMw variance, contributed by both TD and APD variabilities, was large and it strongly increased in HF. The increased variances in the HF model result from an increased sensitivity of the model to perturbations; experiments have also shown a larger APD variability in HF [21–23].

3.2. Rate-dependency of electro-mechanics

Consistent with experimental observations, the response of healthy myocytes to an increase in heart rate was APD shortening and an increase of CaT amplitude (CaTA) to generate a larger developed force (DevF) (Fig. 3), the latter effect defining a positive FFR slope.

In HF, the reverse APD rate-dependency was steeper (Fig. 3A), thus APD difference with healthy myocytes decreased as rate increased. At low frequencies, APD difference between both conditions was so elevated that reflected an increased sensitivity of failing myocytes, with longer APDs, to perturbations [24].

The rate-dependency of CaTA, positive and steep in healthy myocytes, was almost completely lost in HF ones (Fig. 3B). Accordingly, the FFR slope was markedly depressed in HF, with a tendency to become negative between 1.5 and 2 Hz (Fig. 3C). The flat HF DevF curve intersected the healthy one at about 0.7 Hz, suggesting that contractile deficit in failing myocytes may be minimal, or even reversed at very slow rates. A flat curve was also observed with CaTA (Fig. 3B) in failing myocytes but it did not intersect the healthy one; this implies that factors other than Ca^{2+} availability may account for the peculiar rate-dependency of DevF.

At this point, it is important to remark that blunted HF curves in CaT and force were not observed when we used the electrophysiological O'Hara model [25] instead of the most updated ToR-ORd [16] version (Supplementary Fig. S1). One of the main differences between the two AP models is I_{CaL} formulation. In addition, LTCC are distributed between T-tubular and sarcolemmal subspaces

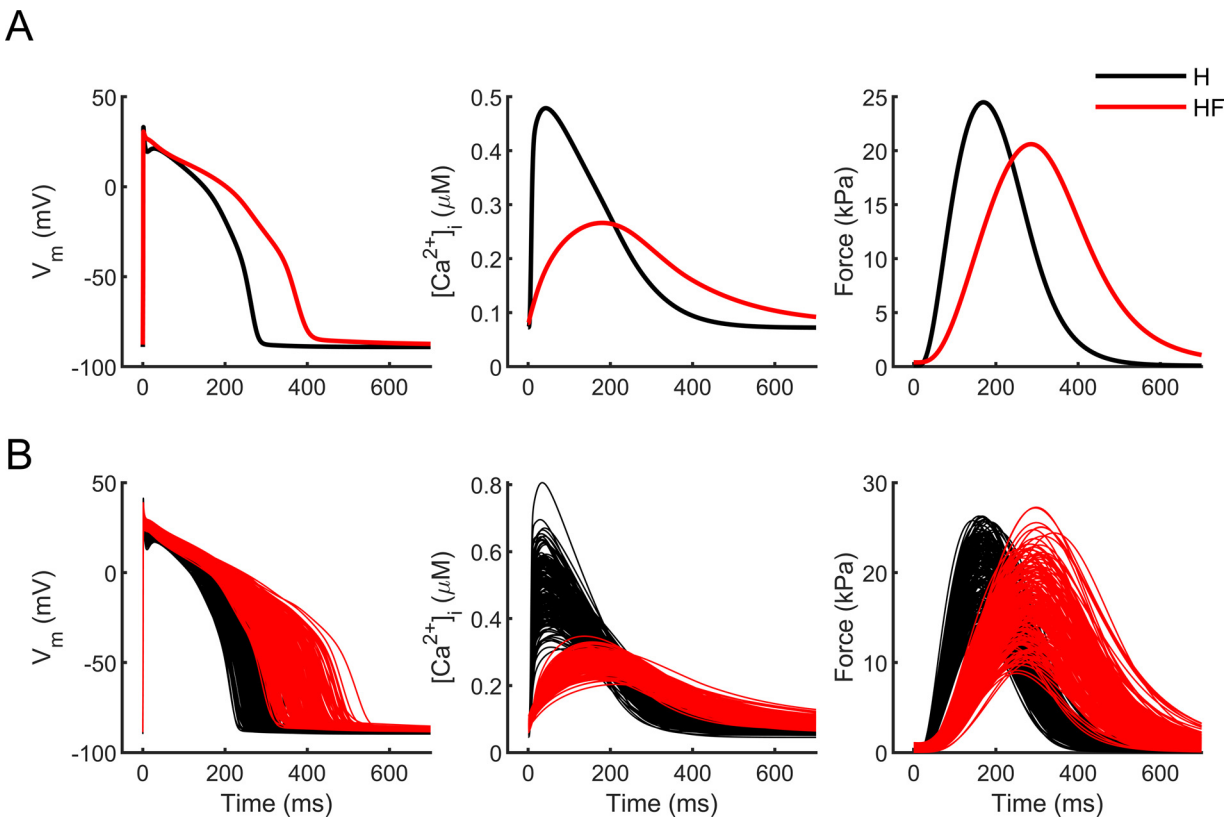

Fig. 1. Comparison between healthy (H) and heart failure (HF) myocytes at 1 Hz for action potential, Ca^{2+} and force transients. A) mean of the two myocyte populations; B) individual myocytes in the two populations.

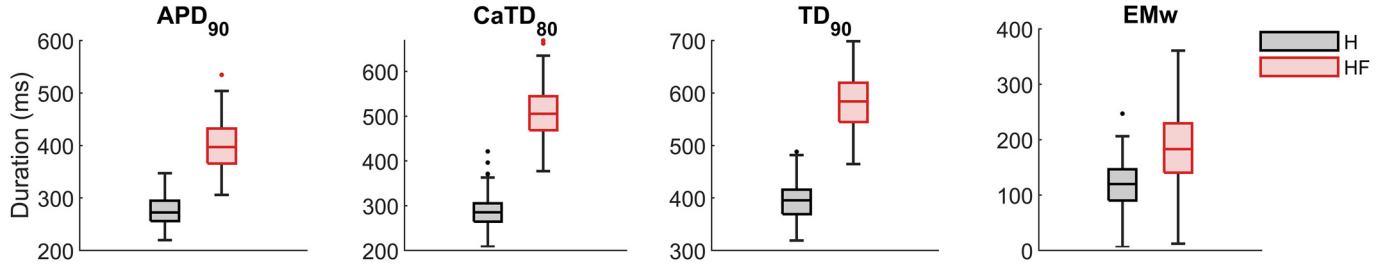

Fig. 2. Comparison of duration intervals in healthy (H) and failing myocytes (HF). Action potential duration (APD_{90}), intracellular Ca^{2+} transient duration ($CaTD_{80}$), total duration of the isometric twitch force (TD_{90}), and electromechanical window (EMw).

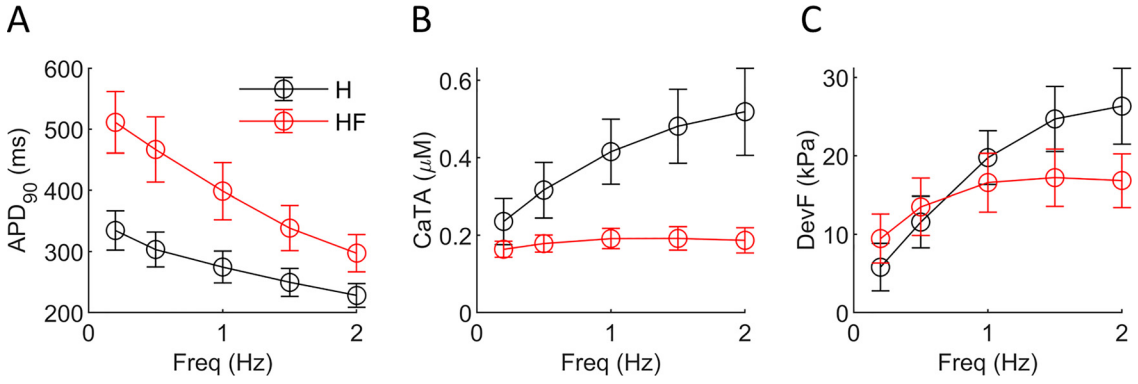

Fig. 3. Rate-dependency in healthy (H) and failing populations of myocytes (HF). A) Action potential duration (APD_{90}), B) Ca^{2+} transient amplitude (CaTA) and C) developed force (DevF) variation with frequency.

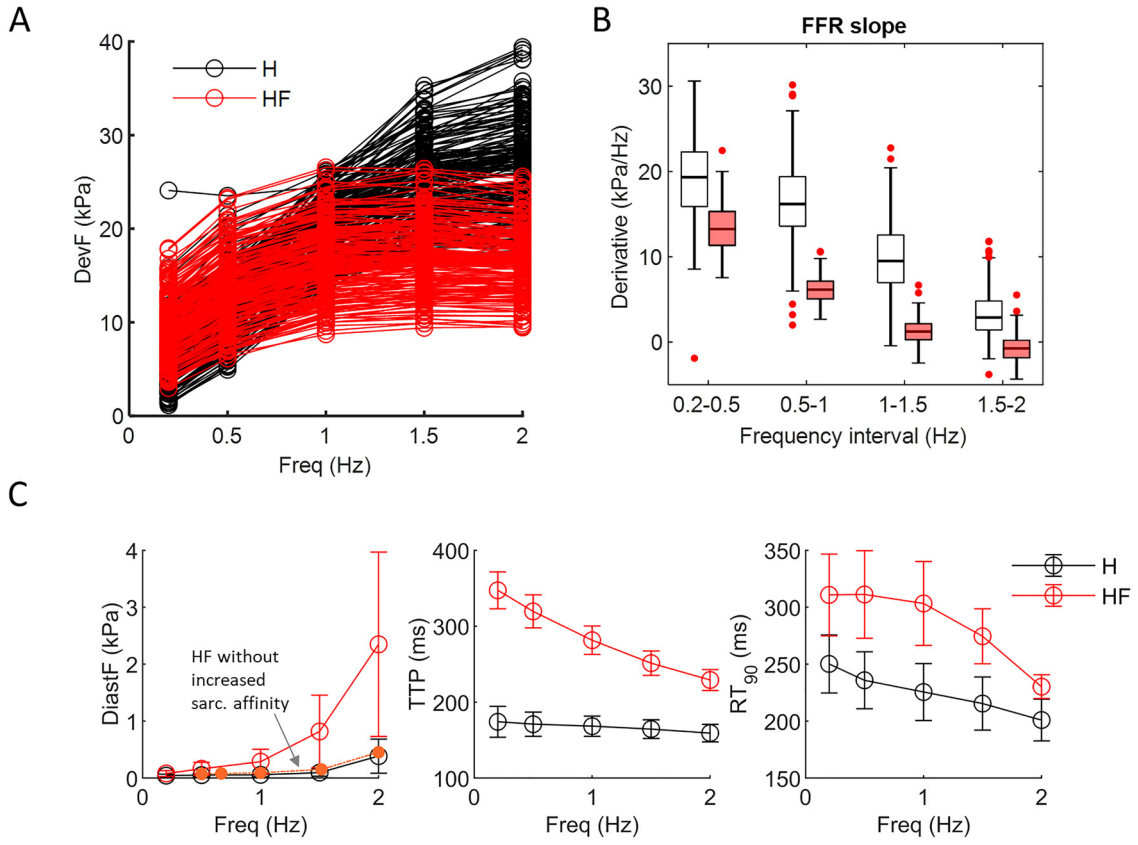

Fig. 4. Impact of frequency on mechanics in the population. A) Force-frequency relationship (FFR) curves of all the cell models, B) Comparison of FFR slopes in frequency intervals between healthy and failing cells. C) Effect of frequency on twitch contraction biomarkers: diastolic force (DiastF), time to peak force (TTP), time from peak force to 90% relaxation (RT_{90}). Data points represent means ± SD of the population of models (H: healthy cells, HF: cells with heart failure).

only in ToR-ORd model, which facilitated the implementation of detubulation for the HF model.

Fig. 4A displays the rate-dependency of DevF of the different cells from the population. Although all the curves essentially reproduced the mean FFR differences between healthy and HF, we can observe the variability in curve steepness in each frequency range. The derivative of the FFR curves ("local" slope) was statistically smaller in HF than in healthy myocytes at all rates with more significant differences at intermediate ones (Fig. 4B). This figure also shows that FFR derivative decreased at higher rates in both populations, as expected from the "saturating" effect of rate; however, saturation was achieved at lower rates in HF.

Diastolic force, the minimum component of DevF, increased with rate (Fig. 4C, left panel) and more steeply in HF. At the highest frequency of stimulation (2 Hz), the marked increase of diastolic force in HF caused an average difference of 2.6 kPa (nine-fold larger) between failing and healthy myocytes. Rate-dependency of diastolic Ca^{2+} was also steeper in HF myocytes (Supplementary Fig. S4), but the difference at 2 Hz amounted to a maximum of 60%. The disproportionate increase of diastolic force at fast rates in HF is the consequence of increased sarcomere Ca^{2+} affinity, as the simulation of HF without the increased sarcomere affinity confirms (Fig. 4C, dotted line). While enhancing contraction at slow rates, the latter may limit Ca^{2+} reuptake by the store and relaxation when diastolic intervals are critically shortened.

Besides DevF, force transient duration parameters were quantified at different rates (Fig. 4C). TTP decreased with rate and the effect was more marked in HF myocytes, which had longer TTP compared to healthy cells. Similarly, RT_{90} was longer in HF and it also decreased with stimulation rate in both myocyte types.

3.3. Mechanisms determining CaTA and DevF changes

To understand the factors underlying the HF-related changes in contraction and its rate-dependency (FFR), we started from the HF model and systematically restored one input parameter at a time to its healthy (pre-remodeling) value. In this analysis we focused on functions relevant to Ca^{2+} handling (SERCA, NCX, RyRs, SR leak, T-tubules and $[Ca]_{T50}$) because CaTA and DevF rate-dependency were correlated. The term "restoration" here means correction of the change induced by HF; i.e. enhancement if function was lost and vice versa.

The effect of some parameters was similar at all rates; other parameters also changed rate-dependency (curve steepness) (Fig. 5). Parameters restoration similarly affected CaTA and DevF (Fig. 5A and B), with the exception of $[Ca]_{T50}$. The latter offset the CaTA curve upward and the DevF one downward, as expected from a decrease in sarcomere Ca^{2+} buffering power and thin-filament activation respectively. To highlight modulation of FFR, curves were normalized for the value at 0.5 Hz (Fig. 5C). SERCA restoration was most effective in recovering CaTA and DevF rate-dependency toward the healthy condition, followed by restoration of NCX and $[Ca]_{T50}$ (Fig. 5C). The effect of restoring other parameters was similar at all rates (no change in slope). T-tubule restoration changed both CaTA and DevF slightly, rate-independently and, unexpectedly, in the negative direction. However, at the dyadic level, CaTA increased and TTP decreased after T-tubule restoration as expected (Supplementary Fig. S5).

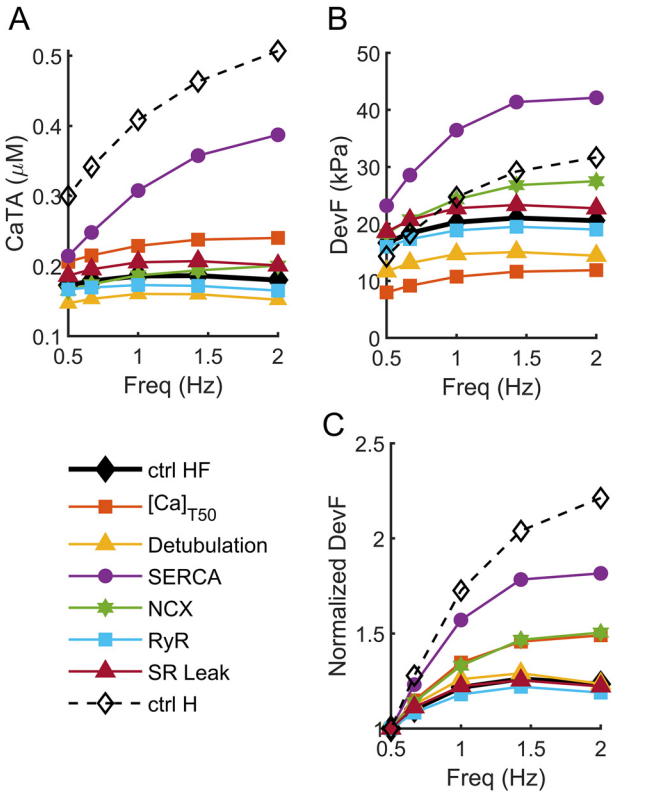

Fig. 5. Modulation of frequency dependency by Ca^{2+} dynamics factors in a failing myocyte. A) intracellular Ca^{2+} transient amplitude (CaTA), B) Force-frequency relationship of absolute developed force (DevF) and C) normalized to DevF at 0.5 Hz. Six parameters were restored, one at a time, taking into account that, in the HF model, myofilament Ca^{2+} sensitivity is increased ($[Ca]_{T50}$ reduction by 30%), 46% of T-tubules are lost, SERCA maximal activity is downregulated by 55%, NCX is upregulated by 60%, RyRs channel sensitivity to SR Ca^{2+} is increased ($K_{rel,Ca}$ reduction by 20%), and Ca^{2+} leak from the SR compartment (SR leak) is increased by 30%.

3.4. Susceptibility to EADs

Under the conditions used to facilitate EADs (dofetilide + low rate), the latter never occurred in the healthy model population. The same conditions induced EADs in 59 out of 190 cells of the HF population. Under these conditions, I_{Kr} was reduced by 40% and parameter variability within the failing population contributed to further decrease the already reduced repolarization reserve in HF and increased EAD vulnerability. Fig. 6A shows the output of the model population; EADs occurred at the transition between phase 2 and 3 of the action potential and were consistently associated with secondary Ca^{2+} and force transients. There were small differences in maximum DevF between cells with and without repolarization abnormalities, but aftercontractions concomitant with EADs might be compromising lusitropy and cellular relaxation.

Myocytes within the HF population were classified in two groups, according to EAD development or not, to compare their input parameters. Whereas sarcomere properties did not differ between the two subpopulations (not shown) a panel of ionic conductances set the conditions for EADs to occur. Fig. 6B compares vulnerable and resistant myocytes to EADs for the scale factors of electrophysiological input parameters because this classification divided each parameter distribution of the population into two new subpopulation distributions (Supplementary Fig. S3). To better explore the difference between groups, a statistical analysis was performed with the Wilcoxon rank sum test by MATLAB and $p < 0.05$ was considered significant. However, as the use of statistical significance tests to interpret simulation results are considered inappropriate, we also focused on the magnitude of the differences observed [26]. Vulnerable myocytes were characterized by significantly larger I_{CaL}, I_{NaL} and NCX, and smaller I_{Kr}, I_{NaK} and SERCA activity.

Whereas the pattern of sarcolemmal conductances in vulnerable myocytes is fully consistent with the notion of reduced repolarization reserve, that reduced SERCA activity should promote EADs was less obvious and raises the question, of therapeutic relevance, of whether SERCA enhancement may be expected to prevent EADs in the context of HF. Thus, we tested whether a 2-fold SERCA enhancement in vulnerable HF myocytes would, on its own, reduce the incidence of EADs. The number of HF models developing EADs was reduced by 71% after increasing SERCA activity by a factor of 2 (Fig. 7A). The incidence and amplitude of secondary force transients (aftercontractions) was consequently reduced. Notably, the amplitude of the main force twitch was barely affected by this level of SERCA enhancement, only a bit smaller and shorter, at least at low stimulation frequencies. At faster heart rates, doubling SERCA increased force as a consequence of the prominent increase in intracellular Ca^{2+} (Supplementary Fig. S6), highlighting that the effect of SERCA modulation is frequency-dependent.

A further question concerns the mechanism by which SERCA enhancement may suppress EADs developed in failing myocytes. To address it, we analyzed in detail the time course of membrane potential, subsarcolemmal (ss, left) and bulk cytosolic (i, right) Ca^{2+} concentrations and relevant membrane currents in one representative HF myocyte before (red) and after (blue) EADs suppression by SERCA enhancement (Fig. 7B). Furthermore, Fig. S8, discussed in the Supplement, shows the contribution of individual fluxes (to and from the cytosol) to the $[Ca^{2+}]_i$ balance at steady-state (total influx=total efflux) in HF myocytes just before the EAD, after the perturbation induced by an EAD and at steady-state after SERCA enhancement (EADs inhibited).

A close analysis of the timing and direction of events during the AP plateau (insets of Fig. 7B) indicates that the EAD was triggered by I_{CaL} reactivation; indeed, the maximal dV/dt of the EAD coincides with the secondary $I_{CaL,ss}$ peak and, because of its outward direction, the I_{NCX} change must be voltage-driven (i.e. an EAD consequence) as opposed to Ca^{2+}-driven.

An increment in SERCA activity enhanced cytosolic Ca^{2+} clearance (decreased $[Ca^{2+}]_i$) and elevated SR Ca^{2+} content (increased $[Ca^{2+}]_{NSR}$), thus boosting the release flux during the action potential plateau. Because of their delayed equilibration, the net effect of SERCA enhancement differed between the two subcompartments: $[Ca^{2+}]_{ss}$ was increased and $[Ca^{2+}]_i$ was decreased. The higher $[Ca^{2+}]_{ss}$ increased the proportion of Ca^{2+}-bound (inactivated) I_{CaL} channels, thus preventing the secondary rise in I_{CaL}. On the other hand, the decrease in $[Ca^{2+}]_i$ reduced forward-mode NCX operation (less inward I_{NCX}) in the non-dyadic sarcolemma. As a consequence of both these events, SERCA enhancement alone abolished I_{CaL} reactivation, and the resulting EAD in a significant proportion of cells.

Despite the comprehensive explanation presented with Fig. 7, the close-loop system hampers the understanding of the real contribution of some parameters. Breaking the loop, possible by means of computer simulations, confirmed the relevant role of I_{CaL}. The I_{CaL} computed with the HF model until the time of EAD takeoff was fed to the SERCA enhanced model and then switched to the usual computation mode. Unlike EAD suppression obtained with SERCA enhancement, clamping a less inactivated I_{CaL} contributed to EAD development (Supplementary Fig. S7).

Myocytes in which the 2-fold SERCA enhancement alone was not enough to suppress EADs had a different protein expression and function than those in which SERCA enhancement had a positive effect. In a first attempt to analyze which parameters contributed to make the cell EAD-prone even after SERCA stimulation,

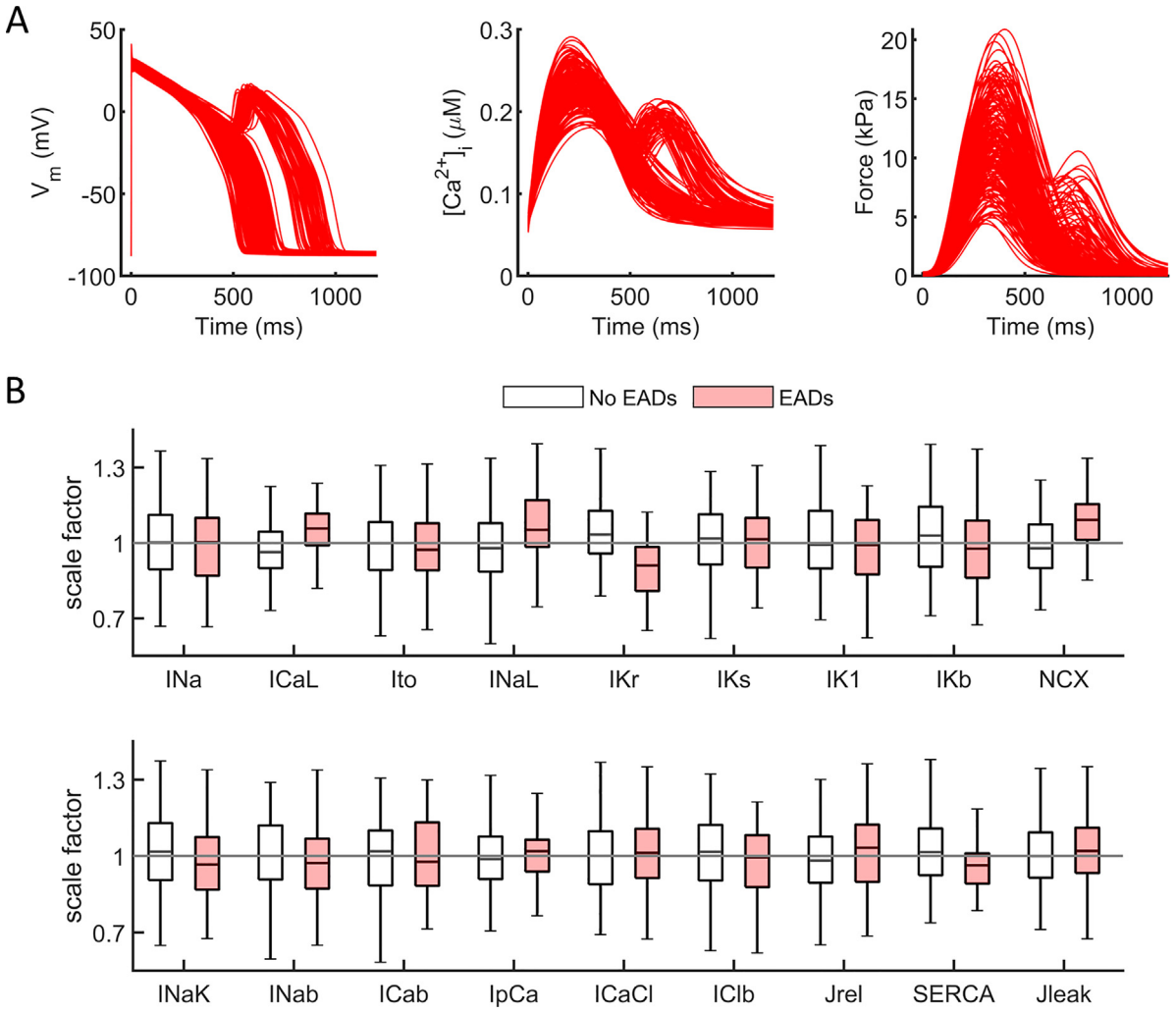

Fig. 6. Effect of 0.01 μM dofetilide on cellular electro-mechanics of the failing population stimulated at 0.25 Hz. A) Action potential, intracellular Ca^{2+} transient (CaT) and force time courses, displaying early afterdepolarizations (EAD) and aftercontractions. B) Comparison between vulnerable (EADs) and resistant (no EADs) myocytes in terms of the scale factors (distributions) applied to the ionic conductances.

no individual parameter stood out as significantly influential; this pointed to the influence of multiple parameter combinations instead. The effect of combinations of parameters on the AP can be assessed by quantifying the "repolarization reserve". To this end, we considered the Q_{Total}/APD ratio which is, by definition, positive (outward) during monotonic repolarization. With the aim to test its predictive power, Q_{Total}/APD was compared between EAD-resistant HF myocytes (without EADs), EAD–vulnerable ones in which SERCA enhancement suppressed EADs (EAD suppression), and those in which EADs persisted even after SERCA enhancement (EADs). Because EADs occurrence would strongly bias the index, in this analysis myocytes were stimulated at 1 Hz and without I_{Kr} block to prevent EADs occurrence in all groups.

Fig. 8 shows that the largest Q_{Total}/APD was in EAD-resistant HF myocytes, the smallest when EADs persisted even after SERCA enhancement and it was intermediate when EADs occurred but could be suppressed by SERCA enhancement.

4. Discussion

4.1. Main findings

This study approaches HF contractile and electrical abnormalities by a model integrating remodeling-induced changes in membrane electricity, intracellular Ca^{2+} dynamics, sarcomere function and disruption of the T-tubule sub-compartment.

Biological variability was reproduced by random scaling of individual input parameters to generate a population of models, each representing a virtual myocyte with properties dictated by the interaction among its unique set of components. This approach allows for robust assessment of the principal determinants of system's response through statistical analysis applied to the population of virtual myocytes.

The average model output reproduced well known features of the failing myocardium, including depressed contraction and slowed relaxation, flat FFR and increased vulnerability to EADs. Systematic recovery of Ca^{2+}-related input parameters identified SERCA depression as the main determinant of FFR flattening in HF, followed by NCX upregulation and increased Ca^{2+} affinity of sarcomeres. SERCA depression (reducing force) and increased Ca^{2+} affinity of sarcomeres (increasing force) were most influential in this condition.

Statistical analysis applied to the population of virtual myocytes allowed to identify which input parameters significantly correlated with EADs vulnerability in HF. As expected, conductance changes leading to an inward shift of the net membrane current at plateau potentials (I_{CaL}, I_{NaL} and I_{NCX} increments, I_{Kr} and I_{NaK} decrements) positively correlated with EADs incidence.

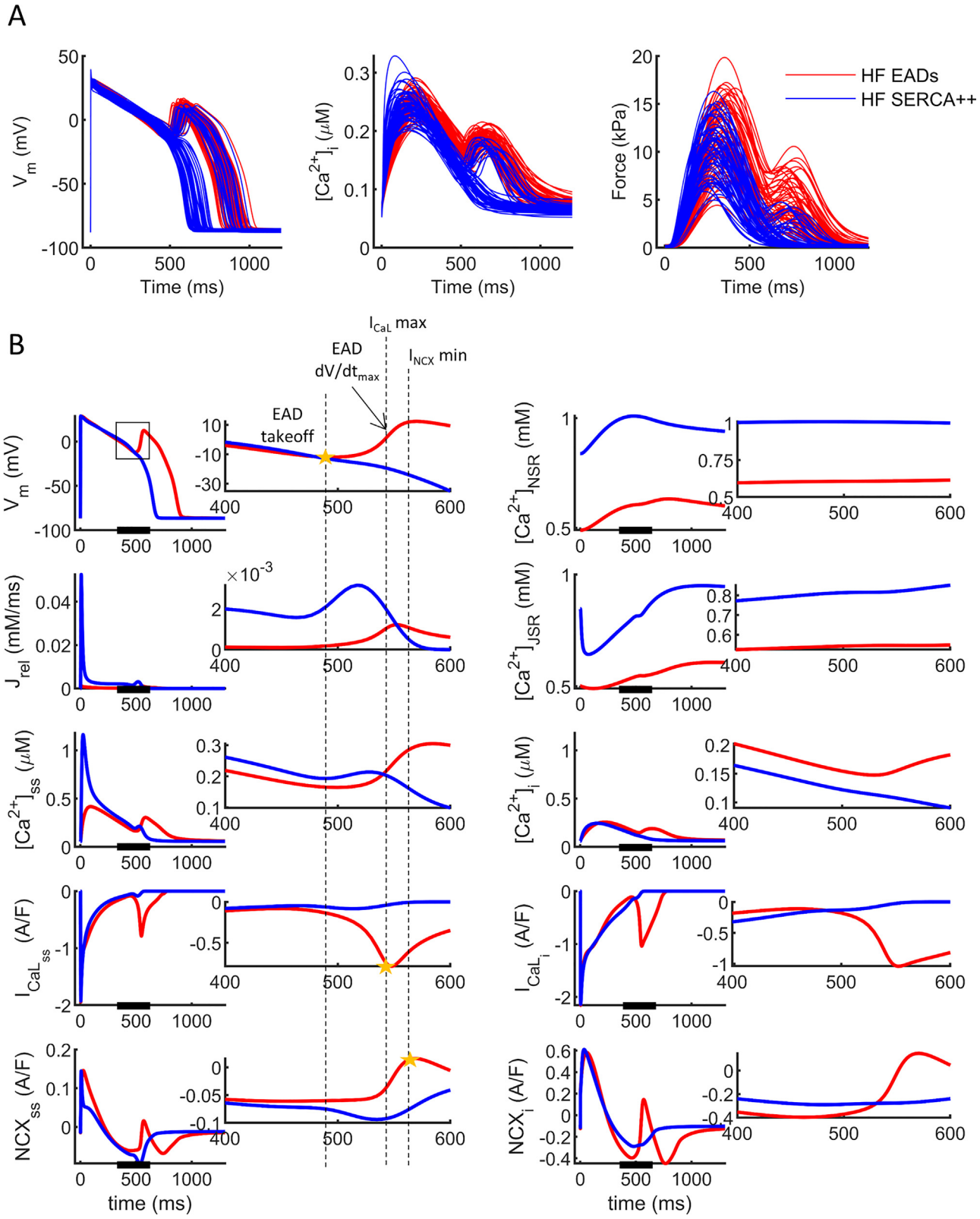

Fig. 7. SERCA enhancement effect on failing cells with early afterdepolarizations (EADs). A) Action potentials (AP) with EADs (first panel) that lead to aftercontractions in Ca^{2+} transient (middle panel) and in twitch force (right panel). Some EADs disappear after 2-fold SERCA enhancement (SERCA++, blue). B) Example of EAD suppression after SERCA enhancement, with changes in AP, currents, Ca^{2+} concentrations and fluxes contributing to repolarization recovery: membrane potential (V_m), intracellular Ca^{2+} concentration ($[Ca^{2+}]$), Ca^{2+} stored in the network and junctional sarcoplasmic reticulum compartments ($[Ca^{2+}]_{NSR}$ and $[Ca^{2+}]_{JSR}$, respectively), SR Ca^{2+} release (J_{rel}), L-type Ca^{2+} current (I_{CaL}) and Na^+/Ca^{2+} exchanger (NCX). Subscripts 'ss' and 'i' refer to the dyadic space (T-tubules) and bulk cytosolic compartment respectively.

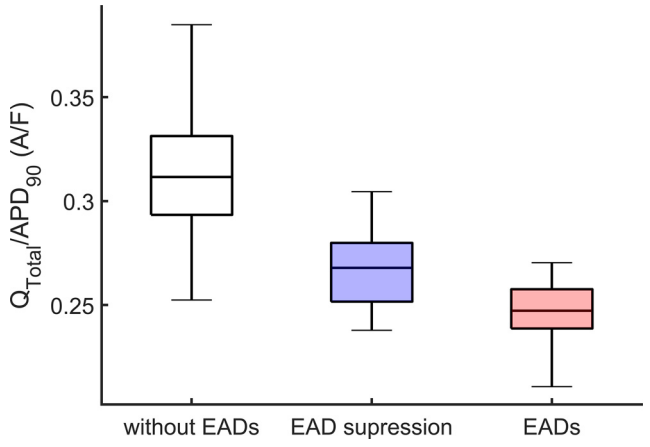

Fig. 8. Comparison of Q_{Total}/APD among the 3 groups of HF cells classified according to their response to SERCA enhancement: those without EADs (left), with EADs suppressed by SERCA enhancement (middle), with persistent EADs (right). Q_{Total}/APD was quantified in "unperturbed" conditions (1 Hz, no I_{Kr} blockade) and before SERCA enhancement.

Less expectedly, SERCA depression was also associated with a larger EADs incidence. The sequence and direction of events just preceding an EAD identifies re-activation of I_{CaL} (in the dyadic space) as the triggering mechanism, Ca^{2+} and I_{NCX} transients being the consequence of membrane depolarization. Recovery of SERCA function increased systolic Ca^{2+} concentration in the dyadic space, thus preventing I_{CaL} re-activation and the consequent EADs. Based on these findings, SERCA enhancement in heart failure provides both electrical and mechanical benefits and we suggest that the development of therapies targeting this protein would be valuable.

4.2. Model validation

The electrophysiological component of the HF model has been validated previously [1,21]; however, the increased complexity introduced by the sarcomeric dynamics and T-tubular changes demands additional validation. The first verification confirmed that the electro-mechanical model in healthy myocytes reproduced rate-dependency of contraction features (DevF, TTP and RT90) fully consistent with measurements in human myocardium [27–29]. Secondly, the HF model reproduced the main features of HF. In terms of electrophysiology an average APD prolongation of 45%, increased APD variability and vulnerability to EADs agreed with experimental observations [21,30]. The aberrant changes in intracellular Ca^{2+} dynamics and force transients were also reproduced [31,32], with an average 50% depression in Ca^{2+} transients and slow kinetics. The model output was quantitatively accurate in terms of force depression (50% to 80% healthy myocytes) but despite changing kinetics accordingly, transient delays could be overestimated [33–36]. Small differences in developed force between healthy and HF myocytes have also been observed and we found that it can occur around 0.7 Hz, where both FFR curves intersect. This crossing between healthy and HF FFR curves at low pacing rates has been experimentally observed in right ventricular tissue and ischemic hearts [29,37].

4.3. Electrophysiological consequences of HF

Repolarization delay is a well-known consequence of myocardial remodeling in HF [38]. Because it tends to increase intracellular Ca^{2+} content, APD prolongation might be seen as compensatory (to the contractile defect); however, it entails a proarrhythmic increase in APD variability [39], in which I_{NaL} is usually involved [40]. This variability, which was clearly captured by the model (Fig. 1), may be largely accounted for by the increase in APD [21]; nonetheless, a contribution of instability in intracellular Ca^{2+} dynamics should be considered [32]. Analyzing such a hypothesis in detail was not among the aims of the present work, however, it may represent a future use of the model.

A decrease (or negativization) in the EMw reportedly correlates with the risk of arrhythmias [15], possibly because of perturbation of the physiological mechano-electric feedback [41]. However, in the present HF model, the EMw was increased instead (i.e., TD_{90} prolonged more than APD_{90}). While EMw shortening has been proposed as a promising biomarker to classify drugs in the torsadogenic risk group, our results imply that conditions promoting EADs may be present in HF even if the EMw positivity is increased. Thus, as an arrhythmia predictor, the EMw might be less sensitive in HF than in primary repolarization abnormalities.

HF patients have a predisposition to develop ventricular arrhythmias, which may end in sudden cardiac death, and EADs are considered a major trigger in their initiation [42,43]. A negative FFR has been associated experimentally to arrhythmias [14], so we took advantage of the results provided by the electro-mechanical HF model to draw conclusions on the cause of EADs.

Because EADs mechanism is not unique, in the present HF model, no initial assumption was made about the mechanisms facilitated by the abnormalities simulating HF. EADs may be primarily "electrical"; i.e., they may reflect the abnormal interplay between membrane potential trajectory (repolarization slowing) and I_{CaL} gating (recovery and reactivation within "window" potentials) [44]. Under some conditions, EADs are associated instead with early spontaneous Ca^{2+} release (SCR) events, thus reflecting SR instability [45].

The timing and direction of events during the AP plateau (insets of Fig. 7B) indicates that the former mechanism supported EADs in this model. Indeed, whereas an SCR-triggered EAD would have been aligned with an inward surge in I_{NCX}, the opposite was true (Fig. 7). The question then arises of which, among HF-associated abnormalities, facilitated I_{CaL} reactivation during the action potential plateau. Fig. 7 inset shows that, just prior to EAD takeoff, repolarization was slightly slowed in HF, but the difference was small; therefore, a faster I_{CaL} recovery from inactivation may also be crucial. An interpretation of its mechanism is suggested by the effects of SERCA enhancement as follows.

I_{CaL} channels largely reside in T-tubules (I_{CaLss}), thus being exposed to the Ca^{2+} levels peculiar of the dyadic space ($[Ca^{2+}]_{ss}$). SERCA enhancement substantially increased SR Ca^{2+} content, CaT amplitude and, thus $[Ca^{2+}]_{ss}$ during the plateau phase (Fig. 7 left panels), agreeing with the well-known role of SERCA on Ca^{2+} homeostasis [46]. This, in turn, delayed the recovery of $I_{CaL,ss}$ from Ca^{2+}-induced inactivation, hence suppressing the EAD. According to this interpretation, SERCA depression, with the resulting reduction of SR Ca^{2+} content, would be an important determinant of EADs vulnerability in HF.

Although still compatible with SERCA depression, events occurring in the non-dyadic intracellular space (Fig. 7 right) are not easily related to EAD triggering. For instance, EAD suppression by SERCA enhancement coincided with lowering of $[Ca^{2+}]_i$ and a sizable increase in I_{CaLi}, both unsuitable to suppress EAD triggering. Nonetheless the reduction in (inward) I_{NCXi} resulting from SERCA enhancement might still contribute to set the stage for EAD suppression. Indeed, it has been pointed out that the generation of EADs in a myocyte may requires two conditions: the presence of a "bistable" behavior of membrane potential plus a triggering "oscillator" [47]. In tissue, either EADs synchronization across multiple cells, or reduced intercellular coupling, is further required to prevent EAD quenching by surrounding myocytes [43]. While I_{CaLss} reactivation accounts for the latter, an inward shift of net membrane

current may add an "equilibrium" point at plateau potentials, as required for membrane potential bistability.

To summarize, at least in the HF setting of the present model, EADs facilitation resulted from: 1) an inward shift of net membrane current (I_{NCXi} and I_{NaL} enhancement, I_{Kr} and I_{NaK} reduction) and 2) premature reactivation of I_{CaLss}. Accordingly, SERCA enhancement may reduce HF EAD incidence by: 1) decreasing I_{NCXi} and 2) enhancing Ca^{2+}-dependent inactivation of I_{CaLss}, both consequences of improved Ca^{2+} compartmentalization within the SR. The antiarrhythmic effect of SERCA enhancement has been previously attributed to improved Ca^{2+} compartmentation within the SR, which may stabilize RyRs and prevent the organization of Ca^{2+} sparks into waves, as reviewed in [48]. Instead of focusing on SR stability, the interpretation suggested by the present results points to modulation of membrane electrophysiology (i.e., increased I_{CaL} inactivation). Both mechanisms may contribute to the antiarrhythmic effect of SERCA enhancement, i.e., the two interpretations are not mutually exclusive.

A 2-fold increase in SERCA activity was not enough to suppress EADs in all cell models, which suggests that suitable combinations of the other HF-induced abnormalities, all concocting to shift Q_{Total}/APD inward, destabilized repolarization beyond reversibility. The correlation between Q_{Total}/APD and EADs inducibility illustrates this concept. Genetic differences in the conductances contributing to mean Q_{Total}/APD may support interindividual variability in arrhythmia susceptibility.

Overall, the analysis of the factors leading to EADs generation and its suppression by SERCA enhancement supports the validity of a conceptual scheme, proposed by Qu et al. [47], borrowed from the theory of non-linear dynamics.

The beneficial effects of SERCA stimulation are known for improving intracellular Ca^{2+} clearance and consequently enhancing contraction [49,50]. Although the analysis of SERCA enhancement did not revealed an increase in force under EAD conditions, other conditions such as an increase in heart rate showed that improvement. Our results suggest additional benefits of SERCA enhancement by reducing ventricular arrhythmias generated by EADs, although restoring deficient SERCA might also reduce arrhythmogenic cardiac alternans as explored by Cutler et al. [51].

4.4. Contractile consequences of HF

As mentioned in the model validation section, the main contractile features of HF were reproduced by the model. Of particular interest is the rate-dependency of developed force (FFR). A positive FFR, observed within physiological ranges in all species and which is more pronounced in large mammals [52], represents the component of cardiac adaptation to stress intrinsic to the myocardium, i.e. independent from neurohumoral regulation. Along with APD shortening, it is important in the preservation of stroke volume at high heart rates [27] and its loss contributes to the HF syndrome [29,37]. The changes responsible for FFR may also lead to an acceleration of the force transient, including its development (TTP) and decay (RT90) [27–29]; all these aspects were reproduced by the healthy myocyte model and were impaired in the HF one. Rate-dependencies of force and force kinetics are not necessarily linked. Indeed, Mashali et al. [29] reported FFR changes but no significant differences in TTP over the whole frequency range nor differences between healthy and failing myocardium. However, TTP differences between detubulated cells and cells with a dense t-system have been experimentally observed [28], which suggests that elevated TTP results from CaT rise delay because of impaired SR Ca^{2+} release provoked by the loss of the T-tubular structure. In fact, we demonstrated by means of computational simulations that FFR is highly related to Ca^{2+} dynamics and that it can be modulated by ionic mechanisms.

Although impaired Ca^{2+} handling and abnormal FFR are clearly related [27], there are still some controversies about the mechanisms primarily involved, which would represent the best targets to restore normal cardiac function in the failing myocardium. This model incorporates all the elements known to be involved in modulating FFR, thus allowing to test their relevance in the HF dysfunction. T-tubules define the dyadic space, where Ca^{2+}-induced I_{CaL} inactivation mostly occurs. The latter, in turn, is crucial in maintaining the Ca^{2+} influx/efflux balance at various rates. RyRs Ca^{2+}-sensitivity sets the gain of EC-coupling. The buffering effect of sarcomeres strongly affects the rates of cytosolic Ca^{2+} clearance and mechanical relaxation, clearly relevant to cope with rate-dependent changes in the electrical and mechanical "duty cycles" (systole/cycle length). The balance between SERCA, leak and NCX fluxes sets the SR Ca^{2+} content and is rate-dependent.

The analysis shown in Fig. 5 allows to identify which among these elements, if restored by therapy, i.e. correction of the change induced by HF, would afford the largest improvement in FFR. Restoration of SERCA activity was most effective in recovering FFR, followed by restoration of NCX and of $[Ca]_{T50}$. Modulation of the other elements changed force development at all rates, but failed to affect FFR appreciably. Cytosolic Ca^{2+} is needed to activate myofilament contraction and SERCA and NCX restoration improved FFR by increasing free cytosolic Ca^{2+}. Although it is known that detubulation alters Ca^{2+} release [53], our results do not highlight recovery of either T-tubules or RyR facilitation as major factors in the recovery of FFR. Notably, this contrasts with experimental observations in rats [54]. The direction of changes fits with logic for all the elements except T-tubules restoration. Whereas the latter was expected to increase CaTA, DevF and restore FRR [54], in the non-dyadic space CaTA was slightly reduced and force (DevF and FFR) remained almost unchanged. However, in the dyadic space T-tubular recovery increased CaTA and shortened TTP, which is more in line with the experimental observations [28,54]. This suggests that the role of the T-tubular dyadic compartment in setting overall myocyte contractile function may be underestimated in the present model. Because the impact of dyadic space crucially depends on the interaction among multiple variables the system response may be difficult to interpret and predict and extrapolate across different species. Thus, while some discrepancies suggest to interpret these particular results with caution, it does not argue against the model predictivity in general.

Rate-dependency of diastolic force has been recently measured in human trabeculae and found to be similar between non-failing and failing muscles [29]. However, our results show a rate-dependent increase in diastolic force in HF as in intracellular Ca^{2+}. Diastolic force build-up at faster heart rates reflects incomplete diastolic relaxation as diastolic time shortens. Two factors, both represented in the model, contribute to rate-dependent diastolic dysfunction: slower Ca^{2+} reuptake into the SR (due to SERCA dysfunction and increased SR leak) and slower Ca^{2+} dissociation from sarcomeres (with increased Ca^{2+} affinity). In agreement with [55,56], our results show elevated diastolic Ca^{2+} due to SERCA downregulation but also due to NCX upregulation, both peculiar of HF remodeling.

4.5. Practical relevance

Possibly the finding of greater practical relevance in the present work is that recovery of SERCA function alone may, albeit through different mechanisms, improve contractile performance and reduce EADs-triggered arrhythmogenesis in the failing heart. However, this finding does not imply that SERCA is the only contributor, as the present study focused on SERCA to exploit the potential of this factor. SERCA enhancement has been initially attempted in HF by gene therapy and failed because of difficulties in construct de-

livery [50]. Nonetheless, recently developed small-molecule SERCA activators are endowed with significant ino-lusitropic effect in acute HF patients [49,57], notably in the absence of proarrhythmia. This provides a realistic opportunity of pharmacological SERCA enhancement.

4.6. Limitations

Active force has been measured under isometric conditions (no sarcomere shortening), thus it represents the maximal force developed at the specified sarcomere length (or maximal elastance, Frank-Starling law). Isometric force has the advantage of being independent of mechanical load, thus allowing direct comparison of data among different experimental settings. However, this approach does not take into account the many consequences of sarcomere shortening, which also contribute to muscle performance during physiological operation. Especially in HF, prestretch effect on force generation and duration may change and the mechano-electrical feedback might show important effects on the EMw at the organ level.

Despite the attempt to model the characteristic detubulation in HF, the approach used showed some flaws in the mechanistic analysis of T-tubules effect. However, the model as a whole firmly reproduced the electromechanical profiles of failing myocytes.

Nonetheless, once validated, a cellular HF electro-mechanical mode can be applied to a wider range of conditions and implemented within tissue and organ models. The latter are required to include the role of passive forces, which largely depend on tissue components providing stiffness (e.g. collagen content) and chamber geometry. Although we did quantify diastolic active force, passive force importantly contributes to diastolic behavior.

Despite these limitations, results of the present study highlighting the benefits of SERCA stimulation are helpful to guide future investigations, especially those targeting SERCA protein to improve cardiac output.

Funding

This work received funding for open access charge: CRUE-Universitat Politècnica de València. The project was supported by the European Union's Horizon 2020 research and innovation programme under grant agreement No 101016496 (SimCardioTest), and by Grant PID2019-104356RB-C41 funded by MCIN/AEI/10.13039/501100011033.

Declaration of Competing Interest

None declared.

Supplementary materials

Supplementary material associated with this article can be found, in the online version, at doi:10.1016/j.cmpb.2023.107350.

References

[1] M.T. Mora, J.M. Ferrero, L. Romero, B. Trenor, Sensitivity analysis revealing the effect of modulating ionic mechanisms on calcium dynamics in simulated human heart failure, PLoS ONE 12 (2017) e0187739, doi:10.1371/journal.pone.0187739.
[2] E. Passini, A. Mincholé, R. Coppini, E. Cerbai, B. Rodriguez, S. Severi, A. Bueno-Orovio, Mechanisms of pro-arrhythmic abnormalities in ventricular repolarisation and anti-arrhythmic therapies in human hypertrophic cardiomyopathy, J. Mol. Cell. Cardiol. 96 (2016) 72–81, doi:10.1016/j.yjmcc.2015.09.003.
[3] J. Llopis-Lorente, J. Gomis-Tena, J. Cano, L. Romero, J. Saiz, B. Trenor, In silico classifiers for the assessment of drug proarrhythmicity, J. Chem. Inf. Model. 60 (2020) 5172–5187, doi:10.1021/acs.jcim.0c00201.
[4] J.J. Rice, F. Wang, D.M. Bers, P.P. De Tombe, Approximate model of cooperative activation and crossbridge cycling in cardiac muscle using ordinary differential equations, Biophys. J. 95 (2008) 2368–2390, doi:10.1529/biophysj.107.119487.
[5] S.A. Niederer, P.J. Hunter, N.P. Smith, A quantitative analysis of cardiac myocyte relaxation: a simulation study, Biophys. J. 90 (2006) 1697–1722, doi:10.1529/biophysj.105.069534.
[6] S. Land, S.-J. Park-Holohan, N.P. Smith, C.G. dos Remedios, J.C. Kentish, S.A. Niederer, A model of cardiac contraction based on novel measurements of tension development in human cardiomyocytes, J. Mol. Cell. Cardiol. 106 (2017) 68–83, doi:10.1016/J.YJMCC.2017.03.008.
[7] E. Pueyo, M. Orini, J.F. Rodríguez, P. Taggart, Interactive effect of beta-adrenergic stimulation and mechanical stretch on low-frequency oscillations of ventricular action potential duration in humans, J. Mol. Cell. Cardiol. 97 (2016) 93–105, doi:10.1016/j.yjmcc.2016.05.003.
[8] J.I. Park, K.M. Lim, Prediction of the mechanical response of cardiac alternans by using an electromechanical model of human ventricular myocytes, Biomed. Eng. Online. 18 (2019) 72, doi:10.1186/s12938-019-0690-x.
[9] A. Hazim, Y. Belhamadia, S. Dubljevic, Effects of mechano-electrical feedback on the onset of alternans: a computational study, Chaos An Interdiscip. J. Nonlinear Sci. 29 (2019) 063126, doi:10.1063/1.5095778.
[10] F. Margara, Z.J. Wang, F. Levrero-Florencio, A. Santiago, M. Vázquez, A. Bueno-Orovio, B. Rodriguez, In-silico human electro-mechanical ventricular modelling and simulation for drug-induced pro-arrhythmia and inotropic risk assessment, Prog. Biophys. Mol. Biol. 159 (2021) 58–74, doi:10.1016/j.pbiomolbio.2020.06.007.
[11] A.R. Lyon, K.T. MacLeod, Y. Zhang, E. Garcia, G.K. Kanda, M.J. Lab, Y.E. Korchev, S.E. Harding, J. Gorelik, Loss of T-tubules and other changes to surface topography in ventricular myocytes from failing human and rat heart, Proc. Natl. Acad. Sci. U. S. A. 106 (2009) 6854–6859, doi:10.1073/pnas.0809777106.
[12] M. Endoh, Force-frequency relationship in intact mammalian ventricular myocardium: physiological and pathophysiological relevance, Eur. J. Pharmacol. 500 (2004) 73–86, doi:10.1016/j.ejphar.2004.07.013.
[13] G. Hasenfuss, C. Holubarsch, H.P. Hermann, K. Astheimer, B. Pieske, H. Just, Influence of the force-frequency relationship on haemodynamics and left ventricular function in patients with non-failing hearts and in patients with dilated cardiomyopathy, Eur. Heart J. 15 (1994) 164–170, doi:10.1093/oxfordjournals.eurheartj.a060471.
[14] D.J. Sprenkeler, A. Bossu, J.D.M. Beekman, M. Schoenmakers, M.A. Vos, An augmented negative force-frequency relationship and slowed mechanical restitution are associated with increased susceptibility to drug-induced torsade de pointes arrhythmias in the chronic atrioventricular block dog, Front. Physiol. 9 (2018), doi:10.3389/fphys.2018.01086.
[15] R.M.A. Ter Bekke, K.H. Haugaa, A. Van Den Wijngaard, J.M. Bos, M.J. Ackerman, T. Edvardsen, P.G.A. Volders, Electromechanical window negativity in genotyped long-QT syndrome patients: relation to arrhythmia risk, Eur. Heart J. 36 (2015) 179–186, doi:10.1093/EURHEARTJ/EHU370.
[16] J. Tomek, A. Bueno-Orovio, E. Passini, X. Zhou, A. Minchole, O. Britton, C. Bartolucci, S. Severi, A. Shrier, L. Virag, A. Varro, B. Rodriguez, Development, calibration, and validation of a novel human ventricular myocyte model in health, disease, and drug block, Elife 8 (2019) 1–47, doi:10.7554/eLife.48890.
[17] J.F. Gomez, K. Cardona, L. Romero, J.M. Ferrero, B. Trenor, Electrophysiological and structural remodeling in heart failure modulate arrhythmogenesis. 1D simulation study, PLoS ONE 9 (2014) e106602, doi:10.1371/journal.pone.0106602.
[18] J.L. Sanchez-Alonso, A. Bhargava, T. O'Hara, A.V. Glukhov, S. Schobesberger, N. Bhogal, M.B. Sikkel, C. Mansfield, Y.E. Korchev, A.R. Lyon, P.P. Punjabi, V.O. Nikolaev, N.A. Trayanova, J. Gorelik, Microdomain-specific modulation of L-type calcium channels leads to triggered ventricular arrhythmia in heart failure, Circ. Res. 119 (2016) 944–945, doi:10.1161/CIRCRESAHA.116.308698.
[19] J. van der Velden, Effect of protein kinase A on calcium sensitivity of force and its sarcomere length dependence in human cardiomyocytes, Cardiovasc. Res. 46 (2000) 487–495, doi:10.1016/S0008-6363(00)00050-X.
[20] P.G. Vikhorev, N.N. Vikhoreva, Cardiomyopathies and related changes in contractility of human heart muscle, Int. J. Mol. Sci. 19 (2018) 2234, doi:10.3390/ijms19082234.
[21] G.-R. Li, C.-P. Lau, T.-K. Leung, S. Nattel, Ionic current abnormalities associated with prolonged action potentials in cardiomyocytes from diseased human right ventricles, Heart Rhythm 1 (2004) 460–468, doi:10.1016/j.hrthm.2004.06.003.
[22] D. Lang, K. Holzem, C. Kang, M. Xiao, H.J. Hwang, G.A. Ewald, K.A. Yamada, I.R. Efimov, Arrhythmogenic remodeling of $\beta 2$ versus $\beta 1$ adrenergic signaling in the human failing heart, Circ. Arrhythmia Electrophysiol. 8 (2015) 409–419, doi:10.1161/CIRCEP.114.002065.
[23] A.V. Glukhov, V.V. Fedorov, Q. Lou, V.K. Ravikumar, P.W. Kalish, R.B. Schuessler, N. Moazami, I.R. Efimov, Transmural dispersion of repolarization in failing and nonfailing human ventricle, Circ. Res. 106 (2010) 981–991, doi:10.1161/CIRCRESAHA.109.204891.
[24] C.K. Antoniou, P. Dilaveris, P. Manolakou, S. Galanakos, N. Magkas, K. Gatzoulis, D. Tousoulis, QT prolongation and malignant arrhythmia: how serious a problem? Eur. Cardiol. Rev. 12 (2017) 112–120, doi:10.15420/ECR.2017:16:1.
[25] T. O'Hara, L. Virág, A. Varró, Y. Rudy, Simulation of the undiseased human cardiac ventricular action potential: model formulation and experimental validation, PLoS Comput. Biol. 7 (2011) e1002061, doi:10.1371/journal.pcbi.1002061.
[26] J.W. White, A. Rassweiler, J.F. Samhouri, A.C. Stier, C. White, Ecologists should not use statistical significance tests to interpret simulation model results, Oikos 123 (2014) 385–388, doi:10.1111/j.1600-0706.2013.01073.x.
[27] B. Pieske, L.S. Maier, D.M. Bers, G. Hasenfuss, Ca2+ handling and sarcoplasmic reticulum Ca2+ content in isolated failing and nonfailing human myocardium, Circ. Res. 85 (1999) 38–46, doi:10.1161/01.RES.85.1.38.
[28] M. Abu-Khousa, D.J. Fiegle, S.T. Sommer, G. Minabari, H. Milting, C. Heim,

M. Weyand, R. Tomasi, A. Dendorfer, T. Volk, T. Seidel, The degree of t-system remodeling predicts negative force-frequency relationship and prolonged relaxation time in failing human myocardium, Front. Physiol. 11 (2020) 182, doi:10.3389/fphys.2020.00182.

[29] M.A. Mashali, N.S. Saad, B.D. Canan, M.T. Elnakish, N. Milani-Nejad, J.H. Chung, E.J. Schultz, S.A. Kiduko, A.W. Huang, A.N. Hare, K.K. Peczkowski, F. Fazlollahi, B.L. Martin, J.D. Murray, C.M. Campbell, A. Kilic, B.A. Whitson, N.A. Mokadam, P.J. Mohler, P.M.L. Janssen, Impact of etiology on force and kinetics of left ventricular end-stage failing human myocardium, J. Mol. Cell. Cardiol. 156 (2021) 7–19, doi:10.1016/J.YJMCC.2021.03.007.

[30] L. Priebe, D.J. Beuckelmann, Simulation study of cellular electric properties in heart failure, Circ Res 82 (1998) 1206–1223, doi:10.1161/01.RES.82.11.1206.

[31] D.J. Beuckelmann, M. Näbauer, E. Erdmann, Intracellular calcium handling in isolated ventricular myocytes from patients with terminal heart failure, Circulation 85 (1992) 1046–1055, doi:10.1161/01.CIR.85.3.1046.

[32] V. Piacentino, C.R. Weber, X. Chen, J. Weisser-Thomas, K.B. Margulies, D.M. Bers, S.R. Houser, Cellular basis of abnormal calcium transients of failing human ventricular myocytes, Circ. Res. 92 (2003) 651–658, doi:10.1161/01.RES.0000062469.83985.9B.

[33] L.A. Mulieri, G. Hasenfuss, B. Leavitt, P.D. Allen, N.R. Alpert, Altered myocardial force-frequency relation in human heart failure, Circulation 85 (1992) 1743–1750, doi:10.1161/01.CIR.85.5.1743.

[34] G.P. Hasenfuss, L.A. Mulieri, B.J. Leavitt, P.D. Allen, J.R. Haeberle, N.R. Alpert, Alteration of contractile function and excitation-contraction coupling in dilated cardiomyopathy, Circ. Res. 70 (1992) 1225–1232, doi:10.1161/01.res.70.6.1225.

[35] B. Pieske, M. Sütterlin, S. Schmidt-Schweda, K. Minami, M. Meyer, M. Olschewski, C. Holubarsch, H. Just, G. Hasenfuss, Diminished post-rest potentiation of contractile force in human dilated cardiomyopathy: functional evidence for alterations in intracellular Ca2+ handling, J. Clin. Invest. 98 (1996) 764–776, doi:10.1172/JCI118849.

[36] C.F. Vahl, T. Timek, A. Bonz, N. Kochsiek, H. Fuchs, L. Schäffer, M. Rosenberg, R. Dillmann, S. Hagl, Myocardial length-force relationship in end stage dilated cardiomyopathy and normal human myocardium: analysis of intact and skinned left ventricular trabeculae obtained during 11 heart transplantations, Basic Res. Cardiol. 92 (1997) 261–270, doi:10.1007/BF00788521.

[37] E.I. Rossman, R.E. Petre, K.W. Chaudhary, V. Piacentino, P.M.L. Janssen, J.P. Gaughan, S.R. Houser, K.B. Margulies, Abnormal frequency-dependent responses represent the pathophysiologic signature of contractile failure in human myocardium, J. Mol. Cell. Cardiol. 36 (2004) 33–42, doi:10.1016/j.yjmcc.2003.09.001.

[38] T. Aiba, G.F. Tomaselli, Electrical remodeling in the failing heart, Curr. Opin. Cardiol. 25 (2010) 29–36, doi:10.1097/HCO.0B013E328333D3D6.

[39] P.P. Nánási, J. Magyar, A. Varró, B. Ördög, Beat-to-beat variability of cardiac action potential duration: underlying mechanism and clinical implications1, doi: 10.1139/Cjpp-2016-0597. 95 (2017) 1230–1235. https://doi.org/10.1139/CJPP-2016-0597.

[40] V.A. Maltsev, N. Silverman, H.N. Sabbah, A.I. Undrovinas, Chronic heart failure slows late sodium current in human and canine ventricular myocytes: implications for repolarization variability, Eur. J. Heart Fail. 9 (2007) 219–227, doi:10.1016/j.ejheart.2006.08.007.

[41] M. Orini, A. Nanda, M. Yates, C. Di Salvo, N. Roberts, P.D. Lambiase, P. Taggart, Mechano-electrical feedback in the clinical setting: current perspectives, Prog. Biophys. Mol. Biol. 130 (2017) 365–375, doi:10.1016/j.pbiomolbio.2017.06.001.

[42] M.J. Janse, Electrophysiological changes in heart failure and their relationship to arrhythmogenesis, Cardiovasc. Res. 61 (2004) 208–217, doi:10.1016/J.CARDIORES.2003.11.018/2/61-2-208-FIG2.GIF.

[43] J.N. Weiss, A. Garfinkel, H.S. Karagueuzian, P.-S. Chen, Z. Qu, Early afterdepolarizations and cardiac arrhythmias, Hear. Rhythm. 7 (2010) 1891–1899, doi:10.1016/J.HRTHM.2010.09.017.

[44] C.T. January, J.M. Riddle, Early afterdepolarizations: mechanism of induction and block. A role for L-type Ca2+ current, Circ. Res. 64 (1989) 977–990, doi:10.1161/01.RES.64.5.977.

[45] Y. Kurata, K. Tsumoto, K. Hayashi, I. Hisatome, Y. Kuda, M. Tanida, Multiple Dynamical Mechanisms of Phase-2 Early Afterdepolarizations in a Human Ventricular Myocyte Model: involvement of Spontaneous SR Ca2+ Release, Front. Physiol. 10 (2020) 1545, doi:10.3389/FPHYS.2019.01545/BIBTEX.

[46] D.M. Bers, Calcium fluxes involved in control of cardiac myocyte contraction, Circ. Res. 87 (2000) 275–281, doi:10.1161/01.RES.87.4.275.

[47] Z. Qu, L.H. Xie, R. Olcese, H.S. Karagueuzian, P.S. Chen, A. Garfinkel, J.N. Weiss, Early afterdepolarizations in cardiac myocytes: beyond reduced repolarization reserve, Cardiovasc. Res. 99 (2013) 6–15, doi:10.1093/cvr/cvt104.

[48] A. Zaza, M. Rocchetti, Calcium store stability as an antiarrhythmic endpoint, Curr. Pharm. Des. 21 (2015) 1053–1061, doi:10.2174/1381612820666141029100650.

[49] M. Rocchetti, M. Alemanni, G. Mostacciuolo, P. Barassi, C. Altomare, R. Chisci, R. Micheletti, P. Ferrari, A. Zaza, Modulation of sarcoplasmic reticulum function by PST2744 [istaroxime; (E,Z)-3-((2-aminoethoxy)imino) androstane-6,17-dione hydrochloride)] in a pressure-overload heart failure model, J. Pharmacol. Exp. Ther. 326 (2008) 957–965, doi:10.1124/jpet.108.138701.

[50] F. del Monte, S.E. Harding, U. Schmidt, T. Matsui, Z.B. Kang, G.W. Dec, J.K. Gwathmey, A. Rosenzweig, R.J. Hajjar, Restoration of contractile function in isolated cardiomyocytes from failing human hearts by gene transfer of SERCA2a, Circulation 100 (1999) 2308–2311, doi:10.1161/01.CIR.100.23.2308.

[51] M.J. Cutler, X. Wan, B.N. Plummer, H. Liu, I. Deschenes, K.R. Laurita, R.J. Hajjar, D.S. Rosenbaum, Targeted sarcoplasmic reticulum Ca2+ ATPase 2a gene delivery to restore electrical stability in the failing heart, Circulation 126 (2012) 2095–2104, doi:10.1161/CIRCULATIONAHA.111.071480.

[52] P.M.L. Janssen, M. Periasamy, Determinants of frequency-dependent contraction and relaxation of mammalian myocardium, J. Mol. Cell. Cardiol. 43 (2007) 523–531, doi:10.1016/J.YJMCC.2007.08.012.

[53] C. Crocini, R. Coppini, C. Ferrantini, P. Yan, L.M. Loew, C. Tesi, E. Cerbai, C. Poggesi, F.S. Pavone, L. Sacconi, Defects in T-tubular electrical activity underlie local alterations of calcium release in heart failure, Proc. Natl. Acad. Sci. U. S. A. 111 (2014) 15196–15201, doi:10.1073/pnas.1411557111.

[54] C. Ferrantini, R. Coppini, L. Sacconi, B. Tosi, M.L. Zhang, G.L. Wang, E. De Vries, E. Hoppenbrouwers, F. Pavone, E. Cerbai, C. Tesi, C. Poggesi, H.E.D.J. Ter Keurs, Impact of detubulation on force and kinetics of cardiac muscle contraction, J. Gen. Physiol. 143 (2014) 783–797, doi:10.1085/jgp.201311125.

[55] A. Baartscheer, C.A. Schumacher, C.N.W. Belterman, R. Coronel, J.W.T. Fiolet, [Na+]i and the driving force of the Na+/Ca2+-exchanger in heart failure, Cardiovasc. Res. 57 (2003) 986–995, doi:10.1016/S0008-6363(02)00848-9.

[56] U. Schmidt, R.J. Hajjar, P.A. Helm, C.S. Kim, A.A. Doye, J.K. Gwathmey, Contribution of abnormal sarcoplasmic reticulum ATPase activity to systolic and diastolic dysfunction in human heart failure, J. Mol. Cell. Cardiol. 30 (1998) 1929–1937, doi:10.1006/jmcc.1998.0748.

[57] V. Carubelli, Y. Zhang, M. Metra, C. Lombardi, G.M. Felker, G. Filippatos, C.M. O'Connor, J.R. Teerlink, P. Simmons, R. Segal, G. Malfatto, M.T. La Rovere, D. Li, X. Han, Z. Yuan, Y. Yao, B. Li, L.F. Lau, G. Bianchi, J. Zhang, Treatment with 24 hour istaroxime infusion in patients hospitalised for acute heart failure: a randomised, placebo-controlled trial, Eur. J. Heart Fail. 22 (2020) 1684–1693, doi:10.1002/EJHF.1743.